Am J Transl Res 2015;7(3):558-573
www.ajtr.org /ISSN:1943-8141/AJTR0004681

Original Article

In vitro comparative study of two decellularization protocols in search of an optimal myocardial scaffold for recellularization

Isaac Perea-Gil[1*], Juan J Uriarte[2,3*], Cristina Prat-Vidal[1], Carolina Gálvez-Montón[1], Santiago Roura[1], Aida Llucià-Valldeperas[1], Carolina Soler-Botija[1], Ramon Farré[2,3,4], Daniel Navajas[2,3,5], Antoni Bayes-Genis[1,6]

[1]ICREC (Heart Failure and Cardiac Regeneration) Research Lab, Health Sciences Research Institute Germans Trias i Pujol (IGTP). Cardiology Service, Hospital Universitari Germans Trias i Pujol, Badalona, Barcelona, Spain; [2]Biophysics and Bioengineering Unit, Faculty of Medicine, University of Barcelona, Barcelona, Spain; [3]CIBER Enfermedades Respiratorias, Madrid, Spain; [4]Institut d'Investigacions Biomèdiques August Pi i Sunyer, Barcelona, Spain; [5]Institute for Bioengineering of Catalonia, Barcelona, Spain; [6]Department of Medicine, Autonomous University of Barcelona (UAB), Barcelona, Spain. [*]Equal contributors.

Received December 10, 2014; Accepted February 8, 2015; Epub March 15, 2015; Published March 30, 2015

Abstract: Introduction. Selection of a biomaterial-based scaffold that mimics native myocardial extracellular matrix (ECM) architecture can facilitate functional cell attachment and differentiation. Although decellularized myocardial ECM accomplishes these premises, decellularization processes may variably distort or degrade ECM structure. Materials and methods. Two decellularization protocols (DP) were tested on porcine heart samples (epicardium, mid myocardium and endocardium). One protocol, DP1, was detergent-based (SDS and Triton X-100), followed by DNase I treatment. The other protocol, DP2, was focused in trypsin and acid with Triton X-100 treatments. Decellularized myocardial scaffolds were reseeded by embedding them in RAD16-I peptidic hydrogel with adipose tissue-derived progenitor cells (ATDPCs). Results. Both protocols yielded acellular myocardial scaffolds (~82% and ~94% DNA reduction for DP1 and DP2, respectively). Ultramicroscopic assessment of scaffolds was similar for both protocols and showed filamentous ECM with preserved fiber disposition and structure. DP1 resulted in more biodegradable scaffolds (P = 0.04). Atomic force microscopy revealed no substantial ECM stiffness changes post-decellularization compared to native tissue. The Young's modulus did not differ between heart layers (P = 0.69) or decellularization protocols (P = 0.15). After one week, recellularized DP1 scaffolds contained higher cell density (236 ± 106 and 98 ± 56 cells/mm^2 for recellularized DP1 and DP2 scaffolds, respectively; P = 0.04). ATDPCs in both DP1 and DP2 scaffolds expressed the endothelial marker isolectin B4, but only in the DP1 scaffold ATDPCs expressed the cardiac markers GATA4, connexin43 and cardiac troponin T. Conclusions. In our hands, DP1 produced myocardial scaffolds with higher cell repopulation and promotes ATDPCs expression of endothelial and cardiomyogenic markers.

Keywords: Myocardial infarction, acellular myocardial scaffold, extracellular matrix, decellularization protocols, recellularization, adipose tissue-derived progenitor cells

Introduction

In 2012, cardiovascular diseases were ranked as the leading cause of death worldwide (3 in every 10 deaths), with coronary heart diseases representing almost half of these deaths [http://www.who.int/mediacentre/factsheets/fs310/en/]. After myocardial infarction (MI), effective treatments are needed to reduce scar formation, enhance cardiac regeneration and improve ventricular remodeling. MI management has evolved dramatically during the past few decades and now includes both drug administration (aspirin, β-blockers, or angiotensin-converting enzyme inhibitors) and the widespread use of coronary angioplasty and stents. However, cardiac function recovers completely only after heart transplantation, which is hindered by heart donor availability and immunological rejection. Stem cells and tissue engineering are emerging as viable additional therapies for conventional cases [1, 2]. Generation of

bioartificial hearts [3, 4], delivery of stem cells with cardiomyogenic or angiogenic potential to the dysfunctional myocardium [5-8], and engineered tissue grafts and myocardial bioprostheses [9-11] are just a few examples of the proposed therapeutical approaches.

Advances in cardiac tissue engineering have enabled the development of myocardial bioprostheses, based on seeding cells onto natural or synthetic three-dimensional (3D) matrices or scaffolds. In this context, scaffold biomaterial choice is a crucial step, as the scaffold must be able to provide functional cell attachment niches and microenvironments resembling the native structural organization and promoting vascularization to ensure nutrients and oxygen supply into the host tissue [12-15]. Although several synthetic matrices have been tested in small animal models [16-22], natural matrices have appeared as promising myocardial scaffolds due to their greater biocompatibility and biodegradability, as their properties are more similar to those of native cardiac tissue [23]. Compared to other natural matrices, myocardial extracellular matrix (ECM), obtained after decellularization procedures, shows better preservation of the original composition, 3D-architecture and ECM microenvironment [4, 24]. These properties make myocardial ECM a suitable scaffold for cell reseeding and subsequent engraftment into damaged myocardium as a cardiac bioprosthesis.

In this study, we generated decellularized porcine myocardial scaffolds using two distinct decellularization protocols. We then characterized the resulting acellular structures at both mechanical and structural levels and determined their biodegradability. We also compared their properties to those of native myocardium to determine whether the ECM architecture and microenvironment were similar in the decellularized and native tissues. Ultimately, the acellular scaffolds were recellularized with porcine adipose tissue-derived progenitor cells (ATDPCs), a cellular lineage with demonstrated mesenchymal stem cell pluripotency and cardiomyogenic and endothelial potential [11].

Materials and methods

Decellularization of porcine myocardial tissue

Cadaveric hearts were obtained from healthy slaughterhouse pigs and immersed in ice-cold phosphate buffer saline (PBS) supplemented with 1% penicillin and streptomycin (P/S) (Gibco) overnight (O/N) at 4°C. The atrium was removed, and the ventricle was transversally excised to obtain five ventricular sections. The apical and basal sections were discarded due to their smaller size. In the three remaining sections, transverse abscission of the lateral wall of left ventricle was performed to obtain three differentiated myocardial blocks (25 mm x 25 mm x 3 mm) corresponding to each of the three differentiated heart layers i.e. epicardium, mid myocardium and endocardium (**Figure 1A**). The basal lamina and endothelial lamina were preserved for the epicardium and endocardium myocardial blocks, respectively. Prior to decellularization, native (non-decellularized) tissue from each heart layer was frozen in liquid nitrogen and stored at -80°C until use. Two decellularization protocols were tested (Figure S1); both were adapted from methods published previously [3, 9, 11].

The decellularization protocol 1, termed DP1, consisted of detergent treatment using 1% SDS (Sigma) for 72 h, followed by 1% Triton X-100 (Sigma) for 48 h, with solution replacement every 24 h. The myocardial scaffolds were then washed 3 times in 24 h using PBS with 1% P/S [3, 11]. This process was repeated once more with an intermediate sterile distilled water wash between the two cycles. After the second cycle, the scaffolds were treated with 0.1 mg/ml DNase I (Roche) in sterile distilled water for 72 h. Finally, the scaffolds were washed (3 x 2 h) with sterile distilled water [3, 11]. DP1 was performed at room temperature (RT) with constant moderate stirring.

The initial step of the decellularization protocol 2, termed DP2, was a treatment with sterile hypertonic (1.1% NaCl (Sigma)) and hypotonic (0.7% NaCl) solutions. The solutions were alternated every 2 h and repeated twice. This step was followed by an enzymatic incubation with 0.05% trypsin supplemented with 0.02% EDTA (Gibco) for 48 h at 37°C with mild agitation, and then by detergent treatment consisting of PBS supplemented with 1% Triton X-100 plus 1% ammonium hydroxide (Alfa Aesar) for 96 h at RT with moderate stirring; all solutions were replaced every 24 h. The enzymatic and detergent incubations were performed twice with sterile distilled water washes between cycles [9]. Finally, the scaffolds were washed with sterile distilled water O/N.

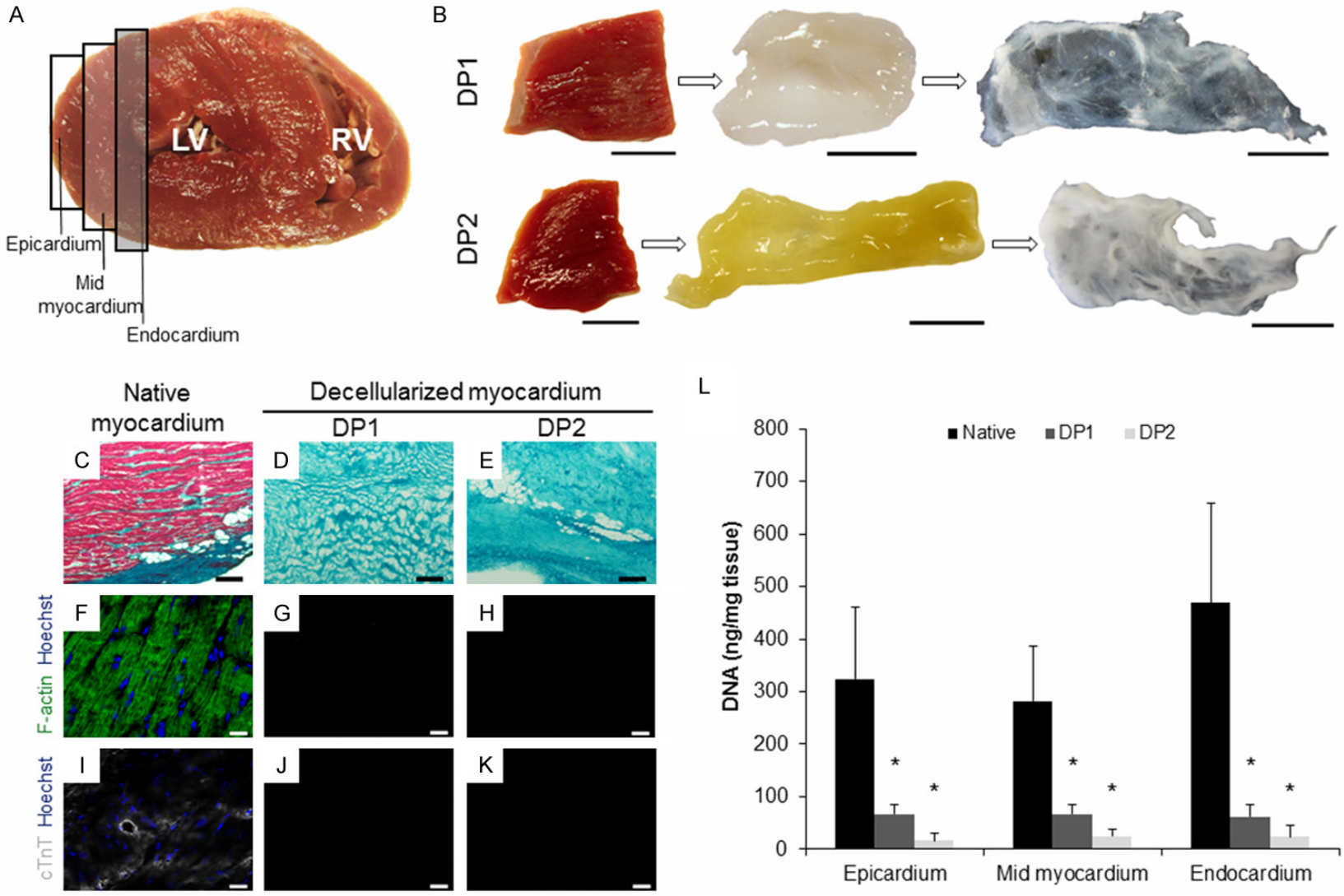

Figure 1. Myocardial tissue decellularization. (A) Transversal excision of ventricle (LV: left ventricle; RV: right ventricle) from porcine heart. LV myocardial samples were obtained from the three heart layers (epicardium, mid myocardium and endocardium), as represented in the figure. (B) Photographs showing each step of DP1 and DP2, respectively: native myocardium sample prior to the decellularization; myocardium after one DP1 or DP2 cycle; and after DP1 or DP2 was completed. Scale bars = 1 cm. (C) Masson's trichrome staining of the native, (D) the DP1-decellularized and (E) the DP2-decellularized myocardium. Collagen fibers are stained light green, and the cytoplasm is stained purple. Scale bars = 200 μm. (F-H) Representative photographs of F-actin (green) and (I-K) cardiac troponin T (cTnT, grey) im-

munostaining for native myocardium, the DP1-treated and the DP2-treated myocardium, respectively. Nuclei were counterstained with Hoechst 33342 (blue). Scale bars = 20 μm. (L) Genomic DNA quantification of the native tissue and decellularized scaffolds for both DP1 and DP2 decellularization protocols and for each of the three heart layers (n = 7). DNA quantity was normalized to the scaffold weight, and data are shown as mean ± SD. *P < 0.001, native myocardium from each heart layer vs. decellularized scaffold.

After completed decellularization procedures, the samples were frozen in liquid nitrogen and stored at -80°C for DNA quantification or stored at 4°C in sterile distilled water plus 1% P/S for further applications.

Lyophilization and sterilization of decellularized scaffolds

Decellularized scaffolds were lyophilized at -23°C for 24 h using a freeze-drier chamber (Christ loc-1 m, B. Braun Biotech International). The lyophilized scaffolds were sterilized under a certified UV dosage of 30 kGy (Aragogamma S.L.) and stored at RT until use.

Histological and immunohistochemical analysis

Native, decellularized myocardial samples and recellularized scaffolds were embedded in TissueTek® OCT compound (Sakura). For primary histological examination, Masson's trichrome (Sigma) and Oil Red O (Sigma) staining were performed on 10 μm sections. Images were taken with an optical microscope (CKX41 Olympus, Olympus).

For immunostaining analysis, decellularized and native myocardium samples were incubated with primary antibodies against type-I collagen (1:100, Abcam), type-III collagen (1:100, Abcam), elastin (1:50, Abcam), Alexa Fluor® 488-conjugated phalloidin for F-actin filament labeling (1:50, Molecular Probes) and cardiac troponin T (1:100, AbD Serotec) followed by incubation with secondary antibodies conjugated to Alexa Fluor® 594 and Alexa Fluor® 488 (1:500, Molecular Probes).

For recellularized myocardial scaffolds, primary antibody labeling was carried out for elastin, biotinylated isolectin B4 (1:50, Vector Labs), GATA4 (1:20, R&D Systems), Alexa Fluor® 488-conjugated phalloidin for F-actin filament labeling, connexin43 (1:100, BD Transduction), and cardiac troponin T. The secondary antibodies were conjugated to Alexa Fluor® 488, Alexa Fluor® 594 and Alexa Fluor® 647 (1:500, Molecular Probes). Nuclei were counterstained with Hoechst 33342 (1:10000, Sigma). Images were captured on a laser confocal microscope (Axio Observer Z1, Zeiss).

DNA quantification

Total genomic DNA was isolated using the PureLink® Genomic DNA kit (Invitrogen) from native myocardium and decellularized scaffolds (n = 7) following the manufacturer's instructions. The total amount of DNA was quantified using spectrophotometry (NanoDrop ND-1000, NanoDrop Technologies) and normalized to the sample tissue weight (average weight: 8.3-24.7 mg).

In vitro assessment of the biodegradability of decellularized scaffolds

Decellularized lyophilized scaffolds (n = 8) were weighed and incubated with 10 ml of a PBS solution containing 0.1% collagenase I (Gibco) for 24 h at 37°C with gentle stirring [25]. Samples were rinsed with sterile distilled water and lyophilized as described above. After 24 h, lyophilized scaffolds were weighed and the percentage of biodegradability (BD) was calculated as previously reported [25].

Scanning electron microscopy (SEM)

Native myocardium and decellularized myocardial scaffolds were washed extensively in sterile distilled water and fixed in 10% formalin O/N at 4°C. The fixed tissue was washed 3 x 10 min with sterile distilled water followed by dehydration with 15 min incubations in increasing ethanol solutions (50%, 60%, 70%, 80%, 90%, and 100% absolute). The dehydrated samples were transferred to a critical point dryer (Emitech Inc.) and dried with CO_2. Samples were sputter-coated with gold using an ion sputter (JFC 1100, JEOL) and visualized at 15 kV with a scanning electron microscopy (JSM-6510, JEOL).

Mechanical testing

Native and decellularized myocardium samples (n = 5) were embedded in TissueTek® OCT com-

pound, and 25 μm-thick slices were thawed at RT and rinsed continuously with PBS until the OCT was completely removed. The slides were then immersed in PBS and placed on the atomic force microscopy (AFM) sample holder.

Stiffness measurements were performed using a custom-built AFM mounted on the stage of an inverted optical microscope (TE2000, Nikon) using a previously described method [26, 27]. The samples were probed with a spherical polystyrene bead of radius R = 2.25 μm attached to a V-shaped gold-coated silicon nitride cantilever with a nominal spring constant k = 0.1 $N \cdot m^{-1}$ (Novascan Technologies). The 3D-cantilever displacement was controlled with sub-nanometer resolution using piezoactuators coupled to strain gauge sensors (Physik Instrumente) that allow measurement of vertical cantilever displacement (z). Cantilever deflection (d) was measured with a quadrant photodiode (S4349, Hamamatsu) using the optical lever method. The slope of a deflection-displacement curve (d-z) obtained on a bare region of the rigid substrate was used to calibrate the relationship between cantilever deflection and photodiode signal. A linear calibration curve with a sharp contact point was taken to indicate a clean undamaged tip. The spring constant was calibrated using the thermal fluctuation method [28]. The force applied by the tip was computed as $F = k \cdot d$.

For each of the three heart layers, local stiffness was measured as follows: for the epicardium, measurements were made 200 μm from the basal lamina edge; for the mid myocardium, measurements were performed in the middle of the sample; and for the endocardium, measurements were made 200 μm from the endothelial lamina edge. In a given region, measurements were performed in 3 locations separated by ~600 μm. At each of the 3 locations, 5 measurements were made separated by ~7 μm; these 5 measurements were taken in a linear or square pattern for native and decellularized samples, respectively. The Young's modulus (E) at each measurement point was computed by recording 5 d-z curves (triangular ramp, peak-to-peak amplitude of 5 μm, and oscillation frequency of 1 Hz) with a maximum indentation of ~1 μm.

Sample indentation (δ) was computed as $\delta = (z\text{-}z_c)\text{-}(d\text{-}d_o)$, where z_c is the displacement of the cantilever at the tip-sample contact point and d_o is the offset of cantilever deflection. Force-indentation data were analyzed using the spherical Hertz model (**Equation 1**) [29]:

$$F = \frac{4ER^{\frac{1}{2}}}{3(1-\mu^{2})}\delta^{\frac{3}{2}} \quad (1)$$

where μ is the Poisson's ratio (assumed to be 0.5). The spherical Hertz model can be expressed in terms of cantilever displacement and deflection as follows:

$$d = d_o \frac{4ER^{1/2}}{3(1-\mu^2)}[z - z_c - (d - d_o)]^{3/2} \quad (2)$$

The Young's modulus, together with z_c and d_o, were computed by least squares fitting of **Equation 2** to the loading phase of the d-z curve using custom-built software (MATLAB, MathWorks). The fitting was performed with a maximum indentation of 0.5 μm to avoid inaccurate z_c determination for shallow indentations and the effect of a rigid substrate for deep indentations [29]. Moreover, to verify that E was not affected by the substrate, force curves recorded in both native and decellularized myocardium were fitted using **Equation 2** by progressively increasing the indentation depth up to 1 μm.

For a given measurement point, E was computed as the average of the values obtained in the 5 d-z curves. The stiffness of each heart region was taken as the average of the E values computed from the fifteen measured points (3 locations x 5 points/location).

Cell culture

Biopsy samples of mediastinal adipose tissue were extracted from juvenile swine and processed to isolate ATDPCs as previously described [30]. ATDPCs were incubated with growth medium: α-MEM (Sigma) medium supplemented with 10% heat-inactivated fetal bovine serum (FBS), 2 mM L-glutamine (Gibco), 1% P/S, and 5 μg/ml Plasmocin™ (Invivogen) under standard culture conditions (37°C, 5% CO_2), with medium replacement every three days.

Recellularization of decellularized scaffolds

Sterile lyophilized decellularized scaffolds (scaffold surface area, 2-2.5 cm^2) were pre-warmed

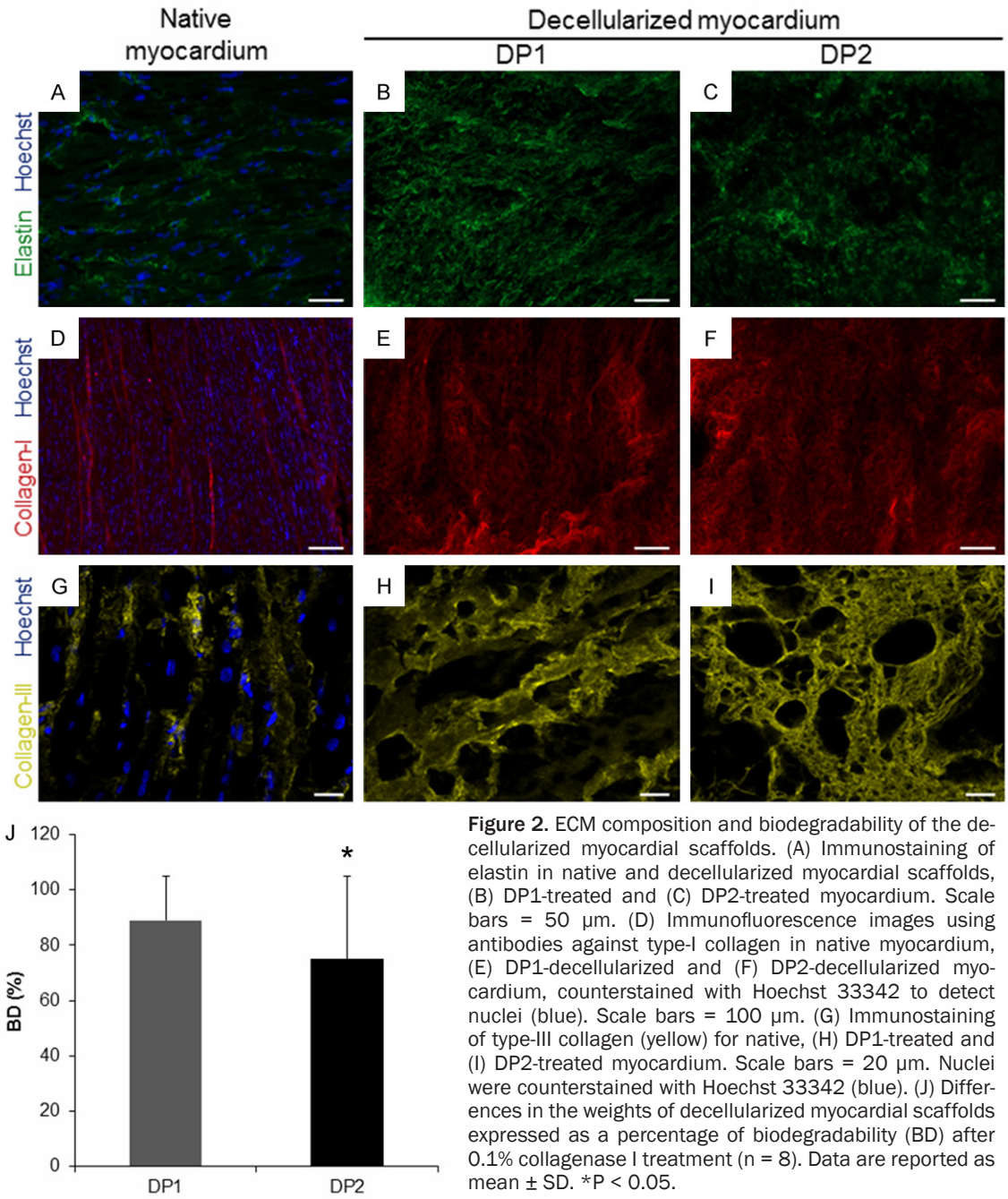

Figure 2. ECM composition and biodegradability of the decellularized myocardial scaffolds. (A) Immunostaining of elastin in native and decellularized myocardial scaffolds, (B) DP1-treated and (C) DP2-treated myocardium. Scale bars = 50 μm. (D) Immunofluorescence images using antibodies against type-I collagen in native myocardium, (E) DP1-decellularized and (F) DP2-decellularized myocardium, counterstained with Hoechst 33342 to detect nuclei (blue). Scale bars = 100 μm. (G) Immunostaining of type-III collagen (yellow) for native, (H) DP1-treated and (I) DP2-treated myocardium. Scale bars = 20 μm. Nuclei were counterstained with Hoechst 33342 (blue). (J) Differences in the weights of decellularized myocardial scaffolds expressed as a percentage of biodegradability (BD) after 0.1% collagenase I treatment (n = 8). Data are reported as mean ± SD. *P < 0.05.

at 37°C in 10-cm diameter plates. Peptidic hydrogel RAD16-I (BD Biosciences) in 0.3% sucrose (Sigma) was sonicated for 5 minutes, and 175 μl of the hydrogel was added to the scaffold. A cellular suspension of 1.75 x 10^6 ATDPCs in 175 μl of 0.22-μm filtered 10% sucrose solution was added onto the scaffolds surface. After 1 hour of incubation under standard culture conditions, growth medium was added to the plates to facilitate RAD16-I hydrogel self-assembly and gel formation. The medium was replaced after 1 h at RT, and the reseeded scaffolds were incubated in standard culture conditions for one week. The medium was replaced every two days.

Cell viability analysis on the recellularized scaffolds

One week post-reseeding, the recellularized scaffolds were washed exhaustively in PBS and

stained using the LIVE/DEAD® Viability/Cytotoxicity Kit (Molecular Probes) following the manufacturer's instructions. Images were acquired using a confocal laser microscope.

Determination of cellular density

Total number of cell nuclei was quantified using ImageJ software (National Institute of Health) in native myocardium and recellularized scaffolds one week post-reseeding (n = 3). At least 5 visual fields were counted for each sample.

Statistical analyses

Data are presented as mean ± SD, and differences among groups were evaluated using the one-way ANOVA and the Tukey post-hoc pairwise multiple comparison tests (SPSS statistics software v.20, IBM). *P* values < 0.05 were considered statistically significant.

Results

Evaluation of myocardial scaffold acellularity

Decellularized myocardial scaffolds were generated using two decellularization protocols (**Figure 1B**). Macroscopically, a single decellularization cycle was not sufficient to obtain completely pale scaffolds for either protocol. After two decellularization cycles, these scaffolds were almost transparent and appeared to be cell-free. There were no notable differences in scaffolds generated from the two protocols or from the three different heart layers.

Histological analysis by Masson's trichrome staining showed no detectable cells remaining in the myocardial scaffolds and no discernable differences between the two protocols or the different heart layers were found (**Figure 1C-E**). Immunostaining revealed absence of cytoskeletal elements and cellular nuclei once myocardium was decellularized (**Figure 1F-K**). In addition, no adipocytes were detected after Oil Red O staining of the myocardial scaffolds (Figure S2).

The DNA content was significantly reduced in the decellularized scaffolds compared to the native myocardium for each of the three heart layers [DNA (ng/mg tissue): epicardium: native = 324 ± 136, DP1 = 67 ± 19, DP2 = 17 ± 14; P < 0.001; mid myocardium: native = 282 ± 106, DP1 = 67 ± 18, DP2 = 26 ± 13; P < 0.001; endocardium: native = 468 ± 190, DP1 = 62 ± 24, DP2 = 23 ± 21; P < 0.001]. The DNA removal efficiency was not significantly different in DP1 vs. DP2 samples (P = 0.31) or in decellularized scaffolds from different heart layers (P = 0.52) (**Figure 1L**). There were thus ~82% and ~94% reductions in the DNA content of the scaffold-associated cells after DP1 and DP2, respectively, compared to native myocardium.

Identification of ECM components and determination of decellularized scaffold biodegradability

Immunostaining showed that type-I, type-III collagen and elastin, characteristic ECM components, were detected in the myocardial scaffolds after both decellularization protocols (**Figure 2A-I**).

Decellularized scaffolds also exhibited high levels of BD as determined by scaffold weight loss after 24 h of collagenase I treatment [BD (%): epicardium: DP1 = 85 ± 17, DP2 = 63 ± 33; mid myocardium: DP1 = 94 ± 13, DP2 = 87 ± 23; endocardium: DP1 = 89 ± 14, DP2 = 75 ± 32]. Even though no significant differences were found between heart layers (P = 0.15), DP1 produced acellular scaffolds that were significantly more biodegradable than those produced after DP2 (P = 0.04) (**Figure 2J**).

Structural and mechanical properties of the acellular scaffolds

Ultrastructural assessment showed decellularized myocardium rich in ECM filaments. Notably, the fiber organization and structure were preserved. In contrast, the scaffolds lacked cardiomyocytes (**Figure 3A-I**), as demonstrated above. No differences were found at ultramicroscopical level between scaffolds generated from the two decellularization protocols or from the different heart layers.

The ECM was easily identified in native myocardium and in decellularized myocardial scaffolds using phase contrast microscopy (**Figure 3J-O**). Mechanical characterization of the ECM using AFM revealed no significant changes in ECM stiffness post-decellularization compared to the native tissue [E (kPa): epicardium: native = 26.1 ± 3.6, DP1 = 28.4 ± 22.3, DP2 = 38.6 ± 20.8; P = 0.51; mid myocardium: native = 30.0

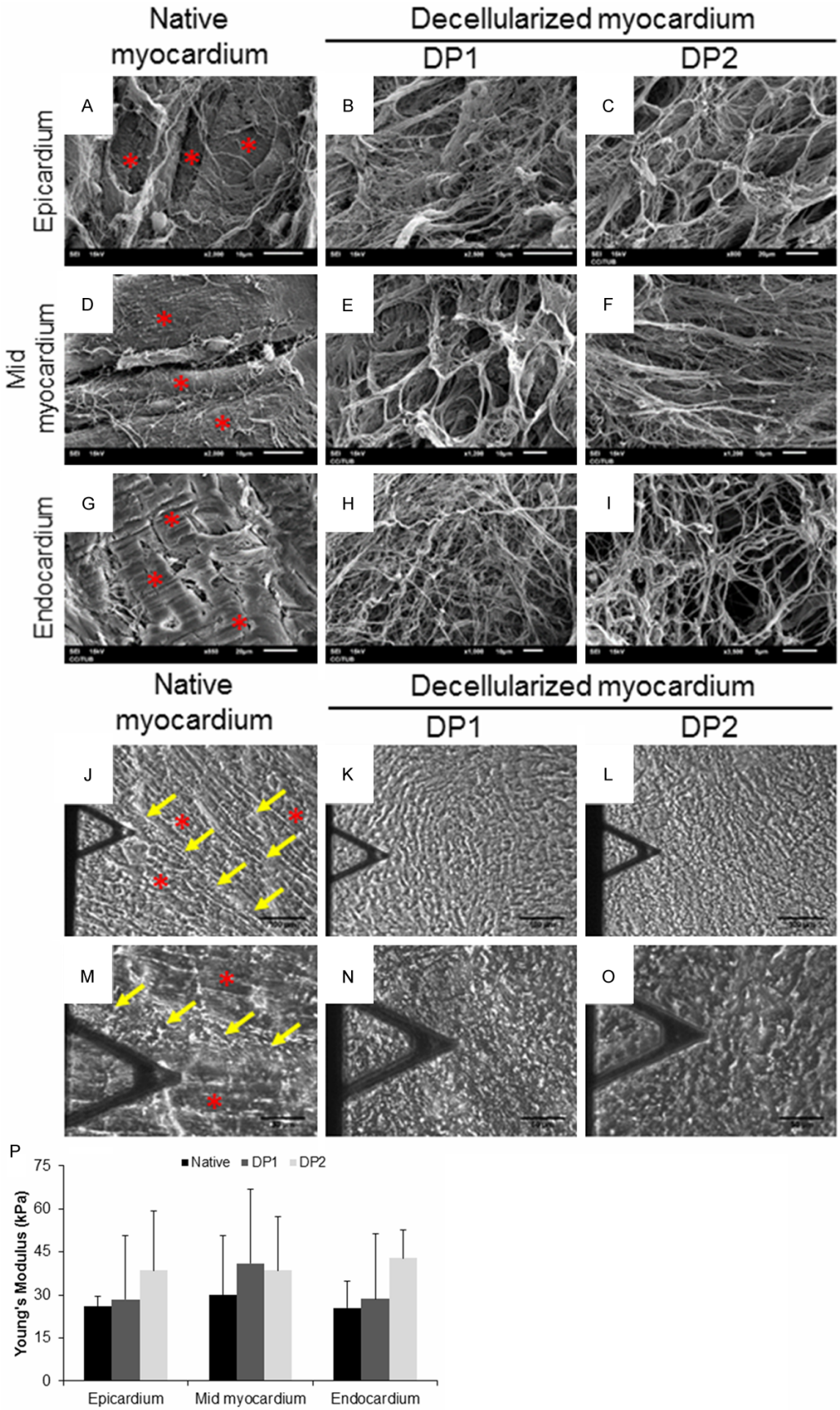
Native myocardium
Decellularized myocardium
DP1
DP2
Epicardium
Mid myocardium
Endocardium
A
B
C
D
E
F
G
H
I
J
K
L
M
N
O
P
Native
DP1
DP2
Young's Modulus (kPa)
75
60
45
30
15
0
Epicardium
Mid myocardium
Endocardium

Figure 3. Structural and mechanical properties of acellular myocardial scaffolds. (A) Scanning electron microscope images of native epicardium, (B) DP1-treated and (C) DP2-treated epicardium; (D) native mid myocardium, (E) DP1-decellularized and (F) DP2-decellularized mid myocardium; (G) native endocardium, (H) endocardium after DP1 treatment and (I) DP2 treatment. (J) Phase contrast images of 25-μm thick slices of myocardium probed with a spherical tip at the end of a V-shaped cantilever by AFM of native myocardium, (K) DP1-decelluarized and (L) DP2-decellularized myocardium. Scale bars = 100 μm. (M) Zoomed images of native myocardium, (N) DP1-decellularized and (O) DP2-decellularized myocardium. Scale bars = 50 μm. Red stars indicate cardiomyocytes. Yellow arrows indicate ECM fibers measured with the AFM. (P) Determination of the Young's modulus ECM, E, for native and decellularized myocardium generated using both decellularization protocols, and for the three heart layers (n = 5). Data are reported as mean ± SD.

± 20.6, DP1 = 41.0 ± 25.7, DP2 = 38.6 ± 18.8; P = 0.71; endocardium: native = 25.5 ± 9.4, DP1 = 28.6 ± 22.9, DP2 = 42.9 ± 10; P = 0.21]. Stiffness was not significantly different in scaffolds from different heart layers (P = 0.69) or in scaffolds generated using DP1 vs. DP2 (P = 0.15) (**Figure 3P**). Thus, the native ECM myocardial stiffness was retained after decellularization.

Recellularization of the decellularized myocardial scaffolds

One week after ATDPCs reseeding within RAD16-I hydrogel onto decellularized myocardial scaffolds, cells were detected inside the scaffold (**Figure 4A-C**) and remained viable as analyzed by live/dead assay (Figure S3). ATDPCs seeded onto scaffolds generated using DP1 and DP2 expressed the endothelial marker isolectin B4 (**Figure 4D**, **4E**). However, only ATDPCs seeded onto scaffolds generated using DP1 expressed the cardiac markers GATA4, connexin43, and cardiac troponin T (**Figure 4D-I**). The capacity of DP1- and DP2-generated scaffolds to retain cells was determined and compared to each other and to the cell density in native myocardium. Cell density was significantly lower in the recellularized scaffolds compared to native myocardium (P < 0.001). Remarkably, recellularized DP1 scaffolds had more cells per surface area than the DP2 (236 ± 106 and 98 ± 56 cells/mm^2 for recellularized DP1 and DP2 decellularized scaffolds, respectively; P = 0.04) (**Figure 4J**).

Discussion

Cardiac tissue engineering is based on placing a mixture of cells with cardioregenerative potential onto a supportive biomaterial. The main challenge in cardiac tissue engineering is finding an optimal biomaterial to serve as a matrix for recellularization in order to generate a bioprosthesis. Matrix composition, its 3D-structure and the microenvironment affect the survival and growth of the reseeded cells and the biomaterial integration success into the host tissue [23, 31]. This challenge can be met using natural myocardial ECM, which is more biodegradable. It is not only a better match than synthetic materials, it also matches the composition and structure of native myocardium better than other natural materials [23]. Notably, the structure and composition of the native ECM constantly varies due to cellular metabolic activity, which in turn causes changes in cell responses to the new ECM environment [32]. These initial microenvironmental cues and normal ECM turnover are only provided by the natural myocardial ECM obtained by decellularization, a mixture of functional and structural molecules which guides cellular proliferation, attachment, differentiation, migration, and viability [33, 34].

To obtain only intact ECM, we need decellularization processes that use physical, enzymatic, and/or chemical treatments to remove all cellular content from the tissue while preserving the integrity of the ECM [2, 35]. Up to date, several organs and tissues have been successfully decellularized, such as heart valves, myocardium, pericardium, lung, pancreas, kidney, liver, mammary gland or nerve [24, 36]. In this study, we chose to test two published decellularization protocols that combine different treatments and to adapt them to our specific conditions. Decellularization treatments used can have a variable effect on ECM: detergents employed, SDS and Triton X-100, can effectively remove cell content, but prolonged exposure could alter ECM ultrastructure and eliminate growth factors. On the other hand, trypsin used in DP2 even though reported to be one of the more commonly used decellularization agents as an initial step, tends to be disruptive to elastin and collagen and ECM ultrastructure, whereas acid treatment of DP2, effective in solubiliz-

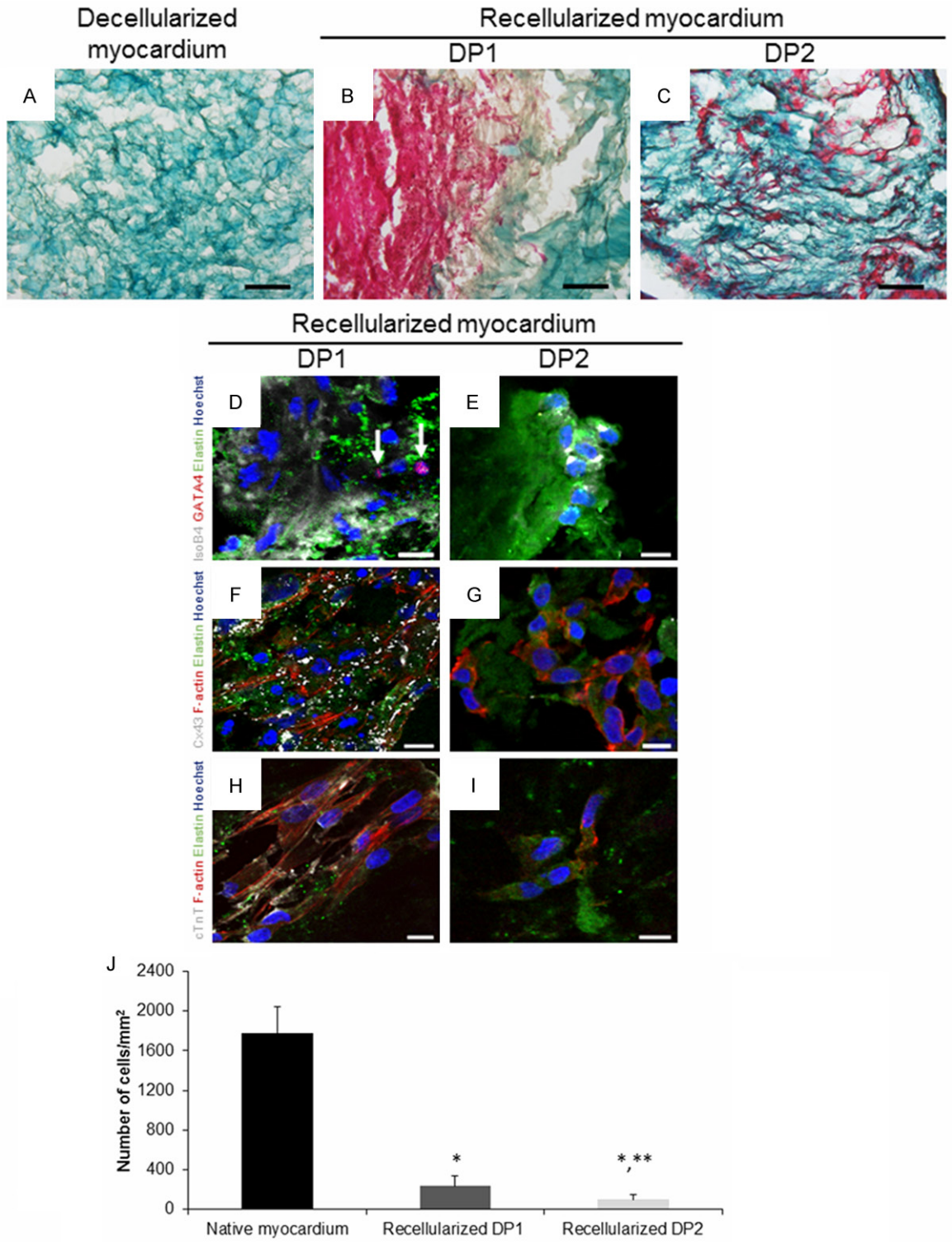

Figure 4. Recellularization of previously decellularized myocardial scaffolds. (A) Representative images of Masson's trichrome staining for decellularized (DP2) myocardial scaffold; (B) DP1- and (C) DP2-decellularized scaffolds one week after recellularization. Collagen fibers are stained light green, and the cytoplasm is stained purple. Scale bars = 100 μm. (D, E) Immunofluorescence against isolectin B4 (IsoB4, grey), GATA4 (red) and elastin (green), (F, G) connexin43 (Cx43, grey) and F-actin (red) and (H, I) cardiac troponin T (cTnT, grey) of DP1- and DP2-decellularized scaffolds, respectively, one week after recellularization with ATDPCs. Nuclei were counterstained with Hoechst 33342 (blue). White arrows indicate cells with positive expression of GATA4. Scale bars = 10 μm. (J) Quantification of cells/mm^2 in native myocardium and in recellularized scaffolds (n = 3). Data are reported as mean ± SD. *P < 0.001, native myocardium vs. recellularized scaffolds; **P < 0.05, DP1- vs. DP2-recellularized scaffolds.

ing cytoplasmatic components and eliminating nucleic acids, could damage collagen, GAGs and remove growth factors. DNase I and hyper/hypotonic treatments have no described negative effects on ECM [24, 36]. Then, we performed a detailed analysis of each decellularization setup for two reasons. First, we wanted to specifically assess the variability of the decellularization effects, which depend on tissue cellularity, origin, density, thickness, lipid content, incubation time, and decellularization technique. Second, we wanted to determine the specific requirements of the cells used for recellularization [24, 37].

Removing cells and nuclear material is necessary to eliminate allogeneic or xenogeneic cell antigens to avoid an adverse immunological host response and graft rejection [38, 39]. It is suggested that a DNA concentration of < 50 ng per mg of scaffold plus no detection of nuclei by immunostaining largely prevents an immunological response [24]. In the present study, we obtained cell-free myocardial scaffolds using two protocols, confirming no presence of cell nuclei in our decellularized scaffolds, and DNA levels were close (DP1) or lower (DP2) than the 50 ng/mg ECM limit, with DNA reduction percentage similar to those obtained in previous work [11, 40]. Additionaly, absence of cytosolic remnants ensures cellular surface molecule α-Gal removal, major factor in the hyperacute rejection of porcine organs transplant [41].

Type-I and III collagen, which contribute mainly to heart stiffness, and elastin, which is involved in cell adhesion and the load-bearing capacity of the heart, are two predominant components of the myocardial ECM [42]. Scaffolds produced by decellularization with DP1 and DP2 were immunopositive for both type-I and III collagen and elastin, indicating that the major ECM components that are needed for subsequent cell reseeding were present.

Regarding biodegradability, an *in vitro* estimation with single enzymatical digestion has been carried out, similarly to those made in previous studies for acellular scaffolds [25, 43-45]. High levels of biodegradability facilitate the replacement of the scaffold ECM by newly-synthetized ECM produced by the reseeded cells. Greater biodegradability thus enhances and promotes the integration of the recellularized scaffold into the engrafted myocardium [35, 42]. Our decellularized scaffolds were highly biodegradable *in vitro*, with the DP1-derived scaffolds being significantly more biodegradable (> 90% for DP1 and > 75% for DP2). Accordingly, our data suggest that it is better to use the DP1 protocol for decellularization. One plausible explanation could be the disruptive effect of trypsin over collagen ultrastructure, which may mask or alter collagenase I cleavage sites, diminishing enzymatic activity on it, as it happens when collagen structure is affected by crosslinking agents [24, 36, 44]. However, these results should be interpreted with caution as an *in vitro* approximation, and degradation kinetics of decellularized scaffolds should be determined *in vivo* once engrafted, according to the high number of metalloproteases involved on ECM degradation [46].

We found that the ECM structure was preserved after decellularization, and microscopic examination showed that the ECM fibers were not only present but that the 3D-organization and ultrastructure were preserved. Conservation of the 3D-ECM ultrastructure post-decellularization facilitates cell adhesion, differentiation, survival, and integration, so ideally the ultrastructure in the scaffold should be similar to that of the native myocardium [23, 24, 33]. The local intrinsic mechanical properties of native and decellularized scaffolds, which are closely related to scaffold structure, were assessed in thin (~25 μm) tissue slices by AFM. This technique has the advantage over bulk mechanical measurements that can directly measure myocardial ECM stiffness in a precisely selected region at a local micro-scale, providing further insights into the cell-microenvironment interconnection [26, 27, 47].

The AFM measurements of the Young's modulus revealed that the local stiffness of the decellularized scaffold is very close to the ECM stiffness in the native myocardium. This suggests that the decellularized scaffold may be able to modulate cell behavior (e.g. cell phenotype, morphology, function, and contractibility) in a manner similar to the modulation that occurs in native tissue [48, 49]. The local stiffness of the decellularized scaffold in the pig myocardium is comparable to that we reported recently in mouse (30-75 kPa) using the same technique [27]. Interestingly, although there are

no other published studies that use AFM in micrometer-thin myocardium slices, similar stiffness values (~20 kPa) were obtained with AFM in thick (0.5-1 mm) native samples of rat [50] and mouse [51] ventricles. Nevertheless, it should be noted that the native myocardium is a composite material with cells embedded in an ECM network. Therefore, indentation of the surface of a thick tissue sample deforms both cells and ECM matrix providing a measurement of the bulk stiffness that depends on the cell-ECM stiffness and volume ratios as wells as scaffold architecture. Other studies have measured bulk mechanical properties of thick (~0.3 mm) myocardial slabs dissected from native rat ventricles and perfused-decellularized hearts by means of biaxial tensile testing [3, 52]. The results for the tangential modulus in the native rat ventricle compare with our Young's modulus measurements in native pig myocardium. By contrast, the tangential modulus of the decellularized rat heart was ~10-fold stiffer than the native tissue [3]. This marked increase in the bulk stiffness of the decellularized tissue can be attributed to decellularization-induced shrinkage and compression of the 3D-ECM network after cell loss. Mechanical properties of native and acellular thick (2-10 mm) slabs of porcine myocardium were also probed with uniaxial testing [9, 10]. Although these studies reported a very high stiffness (220-370 kPa) of the native tissue they also showed a 5- to 20-fold stiffer acellular tissue providing additional evidence of the effect of scaffold shrinkage in tensile assays. Taken together, these data suggest that although the stiffness of the decellularized heart can be altered by changes in the 3D-structure of the ECM network at the macroscopic levels, it is unaffected on the microscopic scale, which is the level at which cardiomyocytes sense mechanical cues from the microenvironment.

We finally characterized the decellularized myocardial scaffolds from each of the heart layers (epicardium, mid myocardium, and endocardium) by examining and comparing several properties. ECM derived from these layers differs in terms of protein composition and in its specific role in the early stages of embryonic heart development [53-55]. Accordingly, we hypothesized that adult heart epicardium and endocardium might have slightly different ECM composition, structure, and/or function than myocardial ECM and that these differences might affect cell reseeding. We found that myocardium from each of the three heart layers showed similar acellularity, ECM proteins detection, ECM biodegradability, 3D-structure and mechanical properties. Consequently, with the decellularization protocols employed, it is suggested that decellularized scaffolds from any of the three heart layers could be used for subsequent cell reseeding, as no differences in ECM characteristics were found.

To date, several types of porcine-derived mesenchymal stem cells have been used for recellularization, including subcutaneous adipose tissue [56], umbilical cord blood [57] and bone marrow [58]. Mediastinal ATDPCs, the porcine mesenchymal stem cells we used for scaffold reseeding, were characterized previously by our group [11]. ATDPCs are pluripotent and express cardiac markers in basal conditions and when cultured in endothelial growth medium, ATDPCs showed endothelial-like morphology and increased isolectin B4 endothelial marker expression, reflecting differentiation towards an endothelial-like cellular lineage [11]. These properties make ATDPCs appropriate to use for scaffold repopulation.

ATDPCs were introduced into the scaffold along with RAD16-I hydrogel, which self-assembles into the matrix and provides an environment that enhances cell viability and cell differentiation towards a cardiac lineage [11, 22, 59]. RAD16-I hydrogel also promotes endothelial cell adhesion and proliferation as well as capillary formation [60]. One week after recellularization, the ATDPCs we observed in the scaffold remained viable and had adhered to the mixture of scaffold plus RAD16-I. ATDPCs expressed isolectin B4 in both DP1- and DP2-decellularized scaffolds, indicating endothelial differentiation potential. Nevertheless, only ATDPCs in DP1-generated scaffolds expressed GATA4, connexin43, and cardiac troponin T, all of which are markers for cardiac lineage differentiation. By mimicking native cardiac ECM or by using decellularized myocardial ECM itself, reseeded cells can be directed to differentiate into mature cardiomyocytes, and in some cases, towards endothelial lineage [4, 61, 62]. Our results indicated that the acellular DP1-generated scaffolds had properties that were more similar to the properties of native ECM.

DP1-generated scaffolds not only promoted ATDPCs endothelial potential, as did DP2-generated scaffolds, but DP1-generated scaffolds also induced cardiac differentiation potential to seeded ATDPCs. Moreover, ATDPCs density was higher for recellularized DP1 scaffolds than for recellularized DP2 scaffolds. Comparing with published data, a similar study recellularized porcine myocardial slabs with 200,000 mesenchymal stem cells seeded onto 0.5 cm^2 of tissue and reported a cell density of 1,000 cells/mm^2 after 30 days [9]. That study started with fewer cells than we did, but the surface area was also smaller. Thus, although they achieved a slightly higher cell density, their results in recellularized porcine myocardium were fairly similar to ours.

Characterization of the decellularized ECM, as well as the recellularization data, indicates that scaffolds decellularized using DP1 were preferable to scaffolds decellularized using DP2. DP1-derived scaffolds were more biodegradable; importantly, they showed a higher density of ATDPCs, and these cells differentially expressed some cardiac markers. All decellularization agents disrupt the scaffold to some extent, but trypsin is more disruptive than other treatments. Prolonged exposure to trypsin can remove ECM elements such as laminin and fibronectin, as well as collagens and elastin (investigated in this study), and GAGs. Acid treatment may remove ECM-bound growth factors [24]. It is difficult to determine the exact exposure time that should be considered as prolonged exposure, i.e. that removes too much of these important ECM proteins and thus alters the ECM microenvironment. Removal of too many key ECM proteins may decrease the number of ATDPCs that adhere to the scaffold and may reduce their expression of cardiac markers as their physiological microenvironment has been altered. Despite trypsin-mediated alterations to the ECM in porcine aortic valves, endothelial cells can grow and proliferate [63]. This suggests that ECM treated with trypsin may still be suitable for endothelial cell proliferation and explains why ATDPCs in DP2-decellularized scaffolds express isolectin B4 but not cardiac markers.

Conclusion

In summary, both decellularization protocols generated acellular myocardial scaffolds with conserved native ECM properties that could be repopulated with ATDPCs. However, decellularized scaffolds obtained with DP1 were more biodegradable and retained more ATDPCs per unit of surface area. Only the ATDPCs reseeded onto DP1-decellularized scaffolds expressed cardiac markers. For these reasons, in our hands, combined use of detergents and DNase, DP1, is an optimal decellularization protocol to obtain acellular scaffolds for recellularization. In the future, these recellularized scaffolds could be enhanced by adding growth factors in order to develop an improved myocardial bioprosthesis.

Acknowledgements

The authors want to thank the members of the Jesús Usón Minimally Invasive Surgery Centre (Cáceres, Spain) for providing mediastinal adipose tissue samples from pigs that underwent cardiothoracic surgery. This work was supported in part by the Instituto de Salud Carlos III: Redes Temáticas de Investigación Cooperativa en Salud [Red de Investigación Cardiovascular (RIC; RD12/0042/0047) and Red de Investigación en Terapia Celular-TerCel (RD12/0019-/0029)] and by Infrastructure Grant (IF09-/3667). The study also received funding from the Ministerio de Ciencia e Innovación (SAF-2011-30067-C02-01/02 to ABG, SAF2011-22576 to RF, FIS-P11/00089 to DN and FIS-PI14/01682); from the Fundació Privada Daniel Bravo Andreu; from La Marató de TV3 (12/2232 to SR); and from the Societat Catalana de Cardiologia and the Sociedad Española de Cardiología.

Address correspondence to: Dr. Antoni Bayes-Genis, ICREC Research Lab, Health Sciences Research Institute Germans Trias i Pujol (IGTP), Cardiology Service, Hospital Universitari Germans Trias i Pujol Crta, Canyet, s/n, 08916 Badalona, Barcelona, Spain. Tel: +34-93-4973743; Fax: +34-93-497865; E-mail: abayesgenis@gmail.com

References

[1] Soler-Botija C, Bagó JR, Bayes-Genis A. A bird's-eye view of cell therapy and tissue engineering for cardiac regeneration. Ann N Y Acad Sci 2012; 1254: 57-65.

[2] Gálvez-Montón C, Prat-Vidal C, Roura S, Soler-Botija C, Bayes-Genis A. Cardiac tissue engineering and the bioartificial heart. Rev Esp Cardiol 2013; 66: 391-399.

[3] Ott HC, Matthiesen TS, Goh SK, Black LD, Kren SM, Netoff TI, Taylor DA. Perfusion-decellularized matrix: using nature's platform to engineer a bioartificial heart. Nat Med 2008; 14: 213-221.
[4] Lu TY, Lin B, Kim J, Sullivan M, Tobita K, Salama G, Yang L. Repopulation of decellularized mouse heart with human induced pluripotent stem cell-derived cardiovascular progenitor cells. Nat Commun 2013; 4: 2307.
[5] Bayes-Genis A, Soler-Botija C, Farré J, Sepúlveda P, Raya A, Roura S, Prat-Vidal C, Gálvez-Montón C, Montero JA, Büscher D, Izpisúa Belmonte JC. Human progenitor cells derived from cardiac adipose tissue ameliorate myocardial infarction in rodents. J Mol Cell Cardiol 2010; 49: 771-789.
[6] Rigol M, Solanes N, Roura S, Roqué M, Novensà L, Dantas AP, Martorell J, Sitges M, Ramírez J, Bayés-Genís A, Heras M. Allogeneic adipose stem cell therapy in acute myocardial infarction. Eur J Clin Invest 2014; 44: 83-92.
[7] Templin C, Zweigerdt R, Schwanke K, Olmer R, Ghadri JR, Emmert MY, Müller E, Küest SM, Cohrs S, Schibli R, Kronen P, Hilbe M, Reinisch A, Strunk D,Haverich A, Hoerstrup S, Lüscher TF, Kaufmann PA, Landmesser U, Martin U. Transplantation and tracking of human-induced pluripotent stem cells in a pig model of myocardium infarction: assessment of cell survival, engraftment, and distribution by hybrid single photon emission computed tomography/computed tomography of sodium iodide symporter transgene expression. Circulation 2012; 126: 430-439.
[8] Kawamoto A, Gwon HC, Iwaguro H, Yamaguchi JI, Uchida S, Masuda H, Silver M, Ma H, Kearney M, Isner JM, Asahara T. Therapeutic potential of ex vivo expanded endothelial progenitor cells for myocardial ischemia. Circulation 2001; 103: 634-637.
[9] Sarig U, Au-Yeung GC, Wang Y, Bronshtein T, Dahan N, Boey FY, Venkatraman SS, Machluf M. Thick acellular heart extracellular matrix with inherent vasculature: Potential platform for myocardial tissue regeneration. Tissue Eng Part A 2012; 18: 2125-2137.
[10] Wang B, Borazjani A, Tahai M, Curry AL, Simionescu DT, Guan J, To F, Elder SH, Liao J. Fabrication of cardiac patch with decellularized porcine myocardial scaffold and bone marrow mononuclear cells. J Biomed Mater Res A 2010; 94: 1100-1110.
[11] Prat-Vidal C, Gálvez-Montón C, Puig-Sanvicens V, Sanchez B, Díaz-Güemes I, Bogónez-Franco P, Perea-Gil I, Casas-Solà A, Roura S, Llucià-Valldeperas A, Soler-Botija C, Sánchez-Margallo FM, Semino CE, Bragos R, Bayes-Genis A. Online monitoring of myocardial bioprosthesis for cardiac repair. Int J Cardiol 2014; 174: 654-661.
[12] Zhou C, Chen J, Sun H, Qiu X, Mou Y, Liu Z, Zhao Y, Li X, Han Y, Duan C, Tang R, Wang C, Zhong W, Liu J, Luo Y, Mengqiu Xing M, Wang C. Engineering the heart: evaluation of conductive nanomaterials for improving implant integration and cardiac function. Sci Rep 2014; 4: 3733.
[13] Dvir T, Timko BP, Kohane DS, Langer R. Nanotechnological strategies for engineering complex tissues. Nat Nanotechnol 2011; 6: 13-22.
[14] Vunjak-Novakovic G, Lui KO, Tandon N, Chien KR: Bioengineering heart muscle: a paradigm for regenerative medicine. Annu Rev Biomed Eng 2011; 13: 245-267.
[15] Song JJ, Ott HC. Organ engineering based on decellularized matrix scaffolds. Trends Mol Med 2014; 17: 424-432.
[16] Jin J, Jeong SI, Shin YM, Lim KS, Shin Hs, Lee YM, Koh HC, Kim KS. Transplantation of mesenchymal stem cells within a poly(lactide-co-ε-caprolactone) scaffold improves cardiac function in a rat myocardial infarction model. Eur J Heart Fail 2009; 11: 147-153.
[17] Miyagi Y, Zeng F, Huang XP, Foltz WD, Wu J, Mihic A, Yau TM, Weisel RD, Li RK. Surgical ventricular restoration with a cell- and cytokine-seeded biodegradable scaffold. Biomaterials 2010; 31: 7684-7694.
[18] Chen QZ, Ishii H, Thouas GA, Lyon AR, Wright JS, Blaker JJ, Chrzanowski W, Boccaccini AR, Ali NN, Knowles JC, Harding SE. An elastomeric patch derived from poly(glycerol sebacate) for delivery of embryonic stem cells to the heart. Biomaterials 2010; 31: 3885-3893.
[19] Siepe M, Giraud MN, Pavlovic M, Receputo C, Beyersdorf F, Menasché P, Carrel T, Tevaearai HT. Myoblast-seeded biodegradable scaffolds to prevent post-myocardial infarction evolution toward heart failure. J Thorac Cardiovasc Surg 2006; 132: 124-131.
[20] Dobner S, Bezuidenhout D, Govender P, Zilla P, Davies N. A synthetic non-degradable polyethylene glycol hydrogel retards adverse post-infarct left ventricular remodeling. J Card Fail 2009; 15: 629-636.
[21] Jiang XJ, Wang T, Li XY, Wu DQ, Zheng ZB, Zhang JF, Chen JL, Peng B, Jiang H, Huang C, Zhang XZ. Injection of a novel synthetic hydrogel preserves left ventricle function after myocardial infarction. J Biomed Mater Res A 2009; 90: 472-477.
[22] Soler-Botija C, Bagó JR, Llucià-Valldeperas A, Vallés-Lluch A, Castells-Sala C, Martínez-Ramos C, Fernández-Muiños T, Chachques JC, Pradas MM, Semino CE, Bayes-Genis A. Engineered 3D bioimplants using elastomeric scaf-

fold, self-assembling peptide hydrogel, and adipose tissue-derived progenitor cells for cardiac regeneration. Am J Transl Res 2014; 6: 291-301.
[23] Sarig U, Machluf M. Engineering cell platforms for myocardial regeneration. Expert Opin Biol Ther 2011; 11: 1055-1077.
[24] Crapo PM, Gilbert TW, Badylak SF. An overview of tissues and whole organ decellularization processes. Biomaterials 2011; 32: 3233-3243.
[25] Kim BS, Choi JS, Kim JD, Choi YC, Cho YW. Recellularization of decellularized human adipose-tissue-derived extracellular matrix sheets with other human cell types. Cell Tissue Res 2012; 348: 559-567.
[26] Luque T, Melo E, Garreta E, Cortiella J, Nichols J, Farré R, Navajas D. Local micromechanical properties of decellularized lung scaffolds measured with atomic forces microscopy. Acta Biomater 2013; 9: 6852-6859.
[27] Andreu I, Luque T, Sancho A, Pelacho B, Iglesias-García O, Melo E, Farré R, Prósper F, Elizalde MR, Navajas D. Heterogeneous micromechanical properties of the extracellular matrix in healthy and infarcted hearts. Acta Biomater 2014; 10: 3235-3242.
[28] Butt HJ, Jaschke M. Calculation of thermal noise in atomic force microscopy. Nanotechnology 1995; 6: 1-7.
[29] Rico F, Roca-Cusachs P, Gavara N, Farré R, Rotger M, Navajas D. Probing mechanical properties of living cells by atomic force microscopy with blunted pyramidal cantilever tips. Phys Rev E Stat Nonlin Soft Matter Phys 2005; 72: 021914.
[30] Martínez-Estrada OM, Muñoz-Santos Y, Julve J, Reina M, Vilaró S. Human adipose tissue as a source of Flk-1^{+} cells: new method of differentiation and expansion. Cardiovasc Res 2005; 65: 328-333.
[31] Grayson WL, Martens TP, Eng GM, Radisic M, Vunjak-Novakovic G. Biomimetic approach to tissue engineering. Semin Cell Dev Biol 2009; 20: 665-673.
[32] Bissell MJ, Aggeler J. Dynamic reciprocity: How do extracellular matrix and hormones direct gene expression? Prog Clin Biol Res 1987; 249: 251-262.
[33] Badylak SF, Taylor D, Uygun K. Whole-organ tissue engineering: decellularization and recellularization of three-dimensional matrix scaffolds. Annu Rev Biomed Eng 2011; 13: 27-53.
[34] Midwood KS, Williams LV, Schwarzbauer TE. Tissue repair and the dynamics of the extracellular matrix. Int J Biochem Cell Biol 2004; 36: 1031-1037.
[35] Robinson KA, Li J, Mathison M, Redkar A, Cui J, Chronos NA, Matheny RG, Badylak S. Extracellular matrix scaffold for cardiac repair. Circulation 2005; 112: 135-143.
[36] Song JJ, Ott HC. Organ engineering based on decellularized matrix scaffolds. Trends in Molecular Medicine 2011; 17: 424-432.
[37] Akhyari P, Aubin H, Gwanmesia P, Barth M, Hoffmann S, Huelsmann J, Preuss K, Lichtenberg A. The quest for an optimized protocol for whole-Heart decellularization: a comparison of three popular and a novel decellularization technique and their diverse effects on crucial extracellular matrix qualities. Tissue Eng Part C Methods 2011; 17: 915-926.
[38] Zheng MH, Chen J, Kirilak Y, Willers C, Xu J, Wood D. Porcine small intestine submucosa (SIS) is not an acellular collagenous matrix and contains porcine DNA: Possible implications in human implantation. J Biomed Mater Res B Appl Biomat 2005; 73: 61-67.
[39] Nagata S, Hanayama R, Kawane K. Autoinmunity and the clearance of dead cells. Cell 2010; 140: 619-630.
[40] Wainwright JM, Czajka CA, Patel UB, Freytes DO, Tobita K, Gilbert TW, Badylak SF. Preparation of cardiac extracellular matrix from an intact porcine heart. Tissue Eng Part C Methods 2010; 16: 525-532.
[41] Badylak SF, Gilbert TW. Immune response to biologic scaffold materials. Semin Immunol 2009; 20: 109-116.
[42] Vunjak Novakovic G, Eschenhagen T, Mummery C. Myocardial tissue engineering: in vitro models. Cold Spring Harb Perspect Med 2014; 4: a014076.
[43] Lu Q, Ganesan K, Simionescu DT, Vyavahare NR. Novel porous aortic elastin and collagen scaffolds for tissue engineering. Biomaterials 2004; 25: 5227-5237.
[44] Liang CH, Chang Y, Hsu CK, Lee MH, Sung HW. Effects of crosslinking degree of an acellular biological tissue on its tissue regeneration pattern. Biomaterials 2004; 25: 3541-3552.
[45] Ma L, Gao C, Mao Z, Zhou J, Shen J. Enhanced biological stability of collagen porous scaffolds by using amino acids as novel cross-linking bridges. Biomaterials 2004; 25: 2997-3004.
[46] Lu P, Takai K, Weaver VM, Werb Z. Extracellular matrix degradation and remodeling in development and disease. Cold Spring Harb Perspect Biol 2011; 3: a005058.
[47] Hersch N, Wolters B, Dreissen G, Springer R, Kirchgeßner N, Merkel R, Hoffmann B. The constant beat: cardiomyocytes adapt their forces by equal contraction upon environmental stiffening. Biol Open 2013; 2: 351-361.
[48] Engler AJ, Carag-Krieger C, Johnson CP, Raab M, Tang HY, Speicher DW, Sanger JW, Sanger JM, Discher DE. Embryonic cardiomyocytes beat best on a matrix with heart-like elasticity:

scar-like rigidity inhibits beating. J Cell Sci 2008; 121: 3794-3802.
[49] Bhana B, Iyer RK, Chen WL, Zhao R, Sider KL, Likhitpanichkul M, Simmons CA, Radisic M. Influence of substrate stiffness on the phenotype of heart cells. Biotechnol Bioeng 2010; 105: 1148-1160.
[50] Berry MF, Engler AJ, Woo YJ, Pirolli TJ, Bish LT, Jayasankar V, Morine KJ, Gardner TJ, Discher DE, Sweeney HL. Mesenchymal stem cell injection after myocardial infarction improves myocardial compliance. Am J Physiol Heart Circ Physiol 2006; 290: H2196-H2203.
[51] Zhang S, Sun A, Ma H, Yao K, Zhou N, Shen L, Zhang C, Zou Y, Ge J. Infarcted myocardium-like stiffness contributes to endothelial progenitor lineage commitment of bone marrow mononuclear cells. J Cell Mol Med 2011; 15: 2245-2261.
[52] Witzenburg C, Raghupathy R, Kren SM, Taylor DA, Barocas VH. Mechanical changes in the rat right ventricle with decellularization. J Biomech 2012; 45: 842-849.
[53] Lockhart M, Wirrig E, Phelps A, Wessels A. Extracellular matrix and heart development. Birth Defects Res A Clin Mol Teratol 2011; 91: 535-550.
[54] Aleksandrova A, Czirók A, Szabó A, Filla MB, Hossain MJ, Whelan PF, Lansford R, Rongish BJ. Connective tissue movements play a major role in avian endocardial morphogenesis. Dev Biol 2012; 362: 348-361.
[55] Trinh LA, Stainier DY. Fibronectin regulates epithelial organization during myocardial migration in zebrafish. Dev Cell 2004; 6: 371-382.
[56] Rigol M, Solanes N, Farré J, Roura S, Roqué M, Berruezo A, Bellera N, Novensà L, Tamborero D, Prat-Vidal C, Huzman MA, Batlle M, Hoefsloot M, Sitges M, Ramírez J, Dantas AP, Merino A, Sanz G, Brugada J, Bayés-Genís A, Heras M. Effects of adipose tissue derived stem cell therapy after myocardial infarction: impact of the route of administration. J Card Fail 2010; 16: 357-366.
[57] Kumar BM, Yoo JG, Ock SA, Kim JG, Song HJ, Kang EJ, Cho SK, Lee SL, Cho JH, Balasubramanian S, Rho GJ. In vitro differentiation of mesenchymal progenitor cells derived from porcine umbilical cord blood. Mol Cells 2007; 24: 343-350.
[58] Ock SA, Jeon BG, Rho GJ. Comparative characterization of porcine mesenchymal stem cells derived from bone marrow extract and skin tissues. Tissue Eng Part C Methods 2010; 16: 1481-1491.
[59] Cui XJ, Xie H, Wang HJ, Guo HD, Zhang JK, Wang C, Tan YZ. Transplantation of mesenchymal stem cells with self-assembling polypeptide scaffolds is conductive to treating myocardial infarction in rats. Tohoku J Exp Med 2010; 222: 281-289.
[60] Sieminski AL, Semino CE, Gong H, Kamm RD. Primary sequence of ionic selfassembling peptide gel affects endothelial cell adhesion and capillary morphogenesis. J Biomed Mater Res Part A 2008; 87: 494-504.
[61] Xu Y, Patnaik S, Guo X, Li Z, Lo W, Butler R, Claude A, Liu Z, Zhang G, Liao J, Anderson PM, Guan J. Cardiac differentiation of cardiosphere-derived cells in scaffolds mimicking morphology of the cardiac extracellular matrix. Acta Biomater 2014; 10: 3449-3662.
[62] Zhang J, Klos M, Wilson GF, Herman AM, Lian X, Raval KK, Barron MR, Hou L, Soerens AG, Yu J, Palecek SP, Lyons GE, Thomson JA, Herron TJ, Jalife J, Kamp TJ. Extracellular matrix promotes highly efficient cardiac differentiation of human pluripotent stem cells: the matrix sandwich method. Circ Res 2013; 111: 1125-1136.
[63] Grauss RW, Hazekamp MG, Oppenhuizen F, van Munsteren CJ, Gittenberger-de Groot AC, DeRuiter MC. Histological evaluation of decellularised porcine aortic valves: matrix changes due to different decellularisation methods. Eur J of Cardiothorac Surg 2005; 27: 566-571.

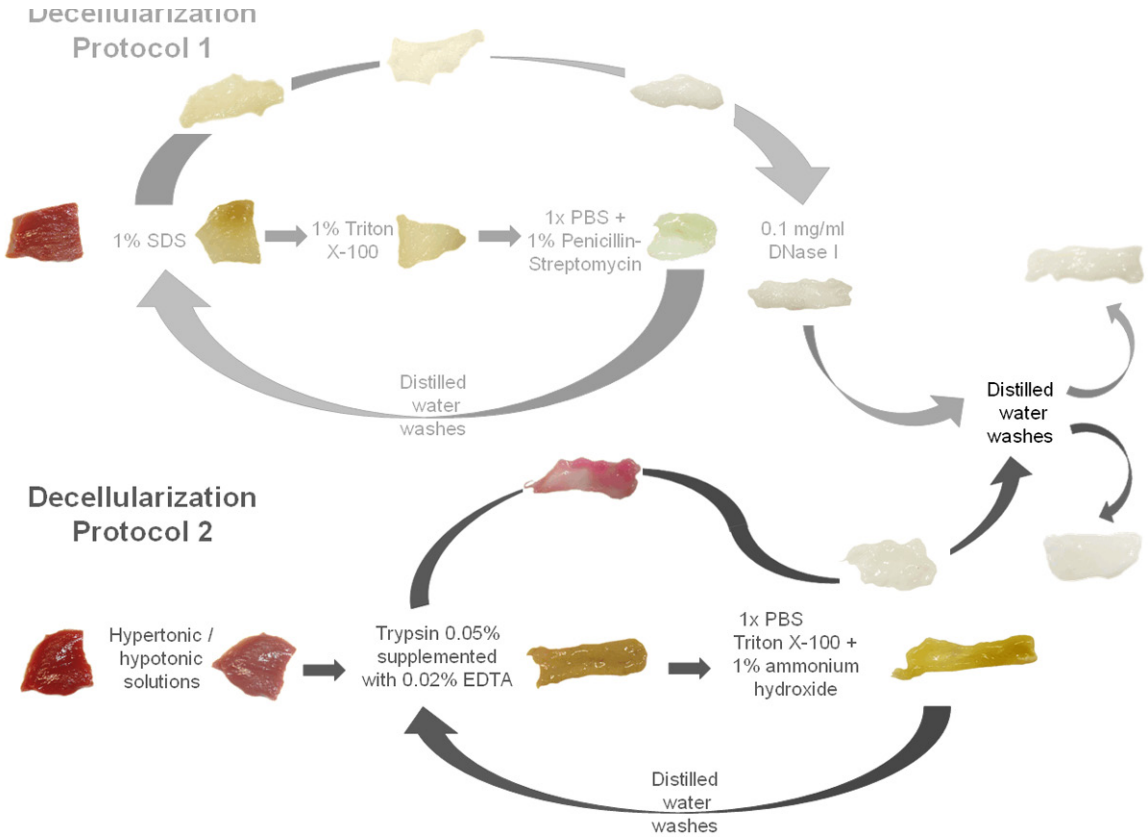

Figure S1. Decellularization protocols at a glance. A schematic view of the decellularization protocols plus photographs taken after each step. DP1 started with 1% SDS treatment for 72 h, followed by Triton X-100 treatment for 48 h, and PBS + 1% penicillin/streptomycin washes. This cycle was repeated again with a distilled water wash between cycles. After the second cycle, samples were treated with 0.1 mg/ml DNase I for 72 h at RT. Finally, the scaffolds were washed 3 times with distilled water (2 h/wash). For DP2, tissue was subjected to hypertonic and hypotonic solutions for 2 h each; this cycle was repeated twice, followed by 0.05% trypsin + 0.02% EDTA for 48 h at 37°C. The solution was replaced after 24 h. Trypsin was replaced by PBS supplemented with 1% Triton X-100 and 1% ammonium hydroxide for 96 h at RT; the solutions were changed every 24 h. Treatment with trypsin and Triton X-100 was repeated with an intermediate wash with distilled water. After the second cycle, the samples were washed with distilled water O/N.

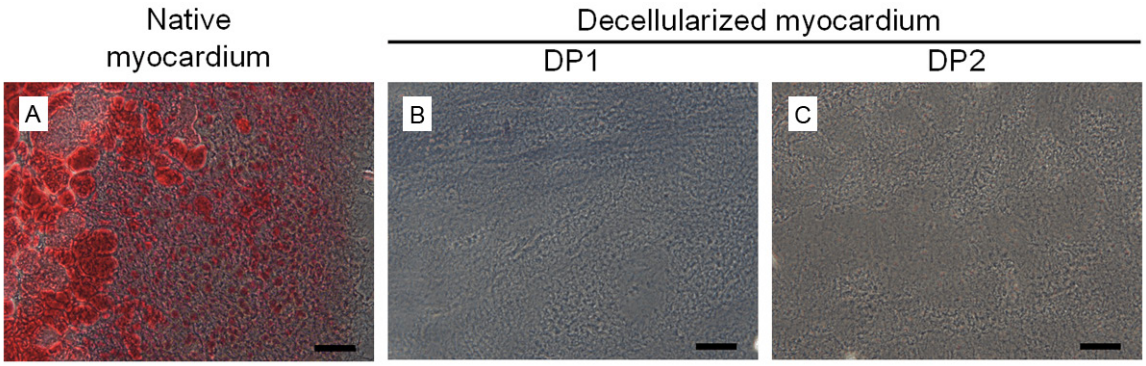

Figure S2. Evaluation of adipocyte remnants in decellularized myocardial scaffolds. (A) Oil Red O staining of native myocardium, (B) DP1-decellularized and (C) DP2-decellularized myocardial scaffolds. Lipid and adipocyte remnants are stained red. Scale bars = 50 µm.

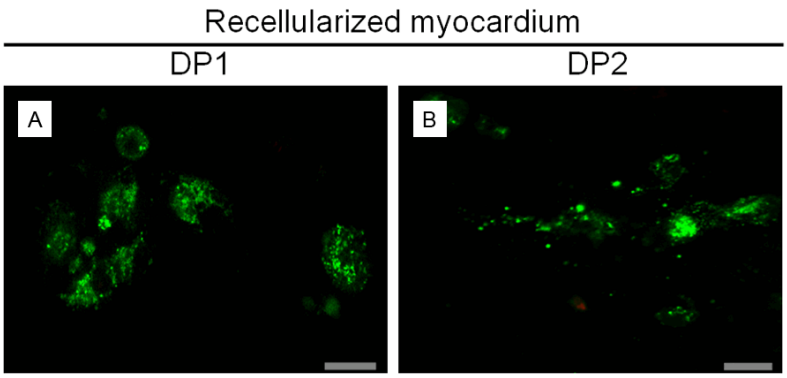

Figure S3. ATDPCs viability assessment in the recellularized scaffolds. (A) LIVE/DEAD® assay to test ATDPCs viability in DP1- and (B) DP2-decellularized scaffolds one week after recellularization (n = 3). Green, live cells; red, dead cells. Scale bars = 20 μm.